

Effects of geometric size and mechanical boundary conditions on magnetoelectric coupling in multiferroic composites

E Pan and R Wang

Computer Modeling and Simulation Group, University of Akron, Akron, OH 44325, USA

E-mail: Pan2@uakron.edu

Received 19 June 2009, in final form 24 September 2009

Published 30 November 2009

Online at stacks.iop.org/JPhysD/42/245503

Abstract

A three-dimensional finite element method program is developed to investigate the magnetoelectric (ME) coupling in multiferroic composites. For a bilayer plate, we show that: (1) the electric potential in the piezoelectric layer induced by the magnetic potential is not uniform but exhibits concentration near the edge/corner of the plate; (2) the mechanically clamped boundary condition can enhance the ME effect by a factor of 10 as compared with the traction-free case; (3) the ME effect in a composite plate is always stronger than that in the corresponding composite beam; (4) a large aspect ratio of the plate corresponds to an increased ME effect; (5) the in-plane longitudinal ME effect is larger than the out-of-plane one.

(Some figures in this article are in colour only in the electronic version)

1. Introduction

A multiferroic material can exhibit an electric polarization under a magnetic field or a magnetization under an electric field, a novel material property which is now called the magnetoelectric (ME) effect. Some single-phase materials exhibit this ME effect but the ME coupling is very weak [1–3]. The strong ME effect was recently observed [4, 5] in artificially fabricated multiferroic composites where the two different-phase materials, i.e. the piezoelectric (PE) and piezomagnetic (PM) single-phase materials, are bonded together. Representative analytical studies on the ME effect include Green's function and perturbation method [6], the micromechanics-based method [7, 8], the equivalent circuit method [9, 10] and the continuum mechanics method with consideration of the grading composition effect [11, 12]. The Stroh formalism and propagator matrix method were also proposed to investigate the full-field response (static and vibration) of the magneto-electro-elastic plates under certain simple lateral mechanical boundary conditions (BCs) [13, 14]. The corresponding ME effect under a harmonic field input, i.e. the ME effect as a function of the input frequency, was also investigated [15, 16]. However, in terms of the ME effect study, most research carried out so far assumed an infinite lateral dimension of the multiferroic composite and as such the effect of the mechanical BCs on the ME coupling was not

considered. This simplification or restriction could be very serious as novel multiferroic composites could be in the fibre-reinforced form [17, 18].

Various numerical methods were proposed to study the multiphase behaviours of multiferroic composites. The layerwise partial mixed finite element method (FEM) was used in [19, 20] to study the static and vibration problems of magneto-electro-elastic layered plates. Similarly, the discrete layer method was employed in [21] for the functionally graded magneto-electro-elastic plates. While the ME effect in the multiferroic composite was investigated in [22] using the FEM method, the FEM was also applied for the composite multiferroic device analysis [23].

In this paper, we develop a three-dimensional (3D) self-contained FEM program to deal with the general and finite-size multiferroic composite structures under arbitrary mechanical BCs. The eight-node brick isoparametric element is adopted and each node in general has five degrees of freedom (DOFs) (three mechanical displacements, one electric potential and one magnetic potential). Both electrode and non-electrode surface conditions can be analysed and the field quantities can be extracted to predict the out-of-plane and in-plane ME effects. Since the assembled stiffness matrix is not positive definite, a special and efficient solver called wave-front [24] is implemented to solve the resulting system of equations. Before applying our 3D FEM program to the ME effect analysis, we

first verified it for the reduced cases by using the commercial FEM software ANSYS (while ANSYS can solve either the PE structure or the PM structure, it cannot treat the problem when all the phases are coupled together). Our FEM program was further tested by other approaches; e.g. we observed that with increasing mesh density, our FEM solutions converge.

2. Basic equations

The general constitutive equation for a magneto-electro-elastic three-phase coupled material can be expressed as [13]

$$\bar{\sigma} = \bar{D}\bar{\gamma}, \quad (1)$$

where

$$\bar{\sigma} = [\sigma \quad D \quad B]^T, \quad (2)$$

$$\bar{\gamma} = [\gamma \quad -E \quad -H]^T, \quad (3)$$

$$\bar{D} = \begin{bmatrix} C & e & q \\ e^T & -\varepsilon & -\alpha \\ q^T & -\alpha^T & -\mu \end{bmatrix} \quad (4)$$

are the extended stress, strain and stiffness vector (matrix) and a superscript T means transpose of the vector (matrix). In these expressions, σ , D and B are vectors of the elastic stress, electric displacement and magnetic induction; γ , E and H are vectors of the elastic strain, electric field and magnetic field; C , e , q , ε , α , μ are matrices of the elastic stiffness (under constant electric and magnetic fields), PE coefficients (under constant strain and magnetic field or under constant electric and magnetic fields), PM coefficients (under constant strain and electric field or under constant electric and magnetic fields), permittivity coefficients (under constant strain and magnetic field), ME coupling coefficients (under constant strain and electric field or under constant strain and magnetic field) and permeability coefficients (under constant strain and electric field). For a layered PE/PM composite where each layer is either PE or PM, the extended stiffness matrix (4) is reduced to

$$\bar{D}_{PE} = \begin{bmatrix} C & e & 0 \\ e^T & -\varepsilon & 0 \\ 0 & 0 & -\mu \end{bmatrix}, \quad (5)$$

$$\bar{D}_{PM} = \begin{bmatrix} C & 0 & q \\ 0 & -\varepsilon & 0 \\ q^T & 0 & -\mu \end{bmatrix} \quad (6)$$

for the PE and PM layers, respectively.

In 3D FEM with eight nodes in each element and five DOFs for each node, the extended strain–displacement equation can be expressed as

$$\bar{\gamma} = \bar{B}\bar{u}, \quad (7)$$

with

$$\bar{u} = (u_1 \quad v_1 \quad w_1 \quad \phi_1 \quad \psi_1 \quad \cdots \quad u_8 \quad v_8 \quad w_8 \quad \phi_8 \quad \psi_8)^T, \quad (8)$$

$$\bar{B} = [B_1 \quad B_2 \quad B_3 \quad B_4 \quad B_5 \quad B_6 \quad B_7 \quad B_8], \quad (9)$$

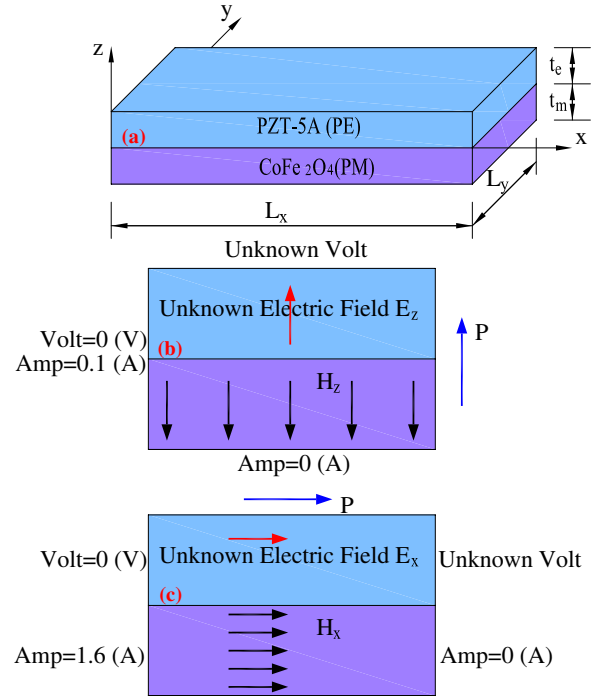


Figure 1. A bilayer PE/PM multiferroic composite plate: geometry in (a), the given electric and magnetic BCs for the out-of-plane longitudinal case in (b) and for the in-plane longitudinal case in (c). The polar direction is also indicated in (b) and (c). (Colour online.)

Table 1. Material properties of PZT-5A (PZT) and CoFe₂O₄ (CFO) [6, 13, 25, 26] (C_{ij} : elastic constants in GPa; e_{ij} : PE coefficients in N (V m)⁻¹; q_{ij} : PM coefficients in N (A m)⁻¹; ε_{ij} : permittivity coefficients in 10⁻⁸ C (V m)⁻¹ and μ_{ij} : permeability coefficients in 10⁻⁶ Wb (A m)⁻¹).

	PZT	CFO		PZT	CFO
C_{11}	99.201	286	q_{13}	0	580.3
C_{12}	54.016	173	q_{23}	0	580.3
C_{13}	50.778	170.5	q_{33}	0	699.7
C_{22}	99.201	286	q_{42}	0	550
C_{23}	50.778	170.5	q_{51}	0	550
C_{33}	86.856	269.5	ε_{11}	1.53	—
C_{44}	21.1	45.3	ε_{22}	1.53	—
C_{55}	21.1	45.3	ε_{33}	1.5	—
C_{66}	22.593	56.5	μ_{11}	—	590
e_{13}	-7.209	0	μ_{22}	—	590
e_{23}	-7.209	0	μ_{33}	—	157
e_{33}	15.118	0			
e_{42}	12.332	0			
e_{51}	12.332	0			

where \bar{u} is a 40×1 extended nodal displacement vector, and each submatrix in \bar{B} can be expressed as

$$[B_i] = \begin{bmatrix} \frac{\partial N_i}{\partial x} & 0 & 0 & 0 & \frac{\partial N_i}{\partial z} & \frac{\partial N_i}{\partial y} & 0 & 0 & 0 & 0 & 0 & 0 & 0 & 0 & 0 \\ 0 & \frac{\partial N_i}{\partial y} & 0 & \frac{\partial N_i}{\partial z} & 0 & \frac{\partial N_i}{\partial x} & 0 & 0 & 0 & 0 & 0 & 0 & 0 & 0 & 0 \\ 0 & 0 & \frac{\partial N_i}{\partial z} & \frac{\partial N_i}{\partial y} & \frac{\partial N_i}{\partial x} & 0 & 0 & 0 & 0 & 0 & 0 & 0 & 0 & 0 & 0 \\ 0 & 0 & 0 & 0 & 0 & 0 & \frac{\partial N_i}{\partial x} & \frac{\partial N_i}{\partial y} & \frac{\partial N_i}{\partial z} & 0 & 0 & 0 & 0 & 0 & 0 \\ 0 & 0 & 0 & 0 & 0 & 0 & 0 & 0 & 0 & 0 & \frac{\partial N_i}{\partial x} & \frac{\partial N_i}{\partial y} & \frac{\partial N_i}{\partial z} & 0 & 0 \end{bmatrix}^T, \quad (10)$$

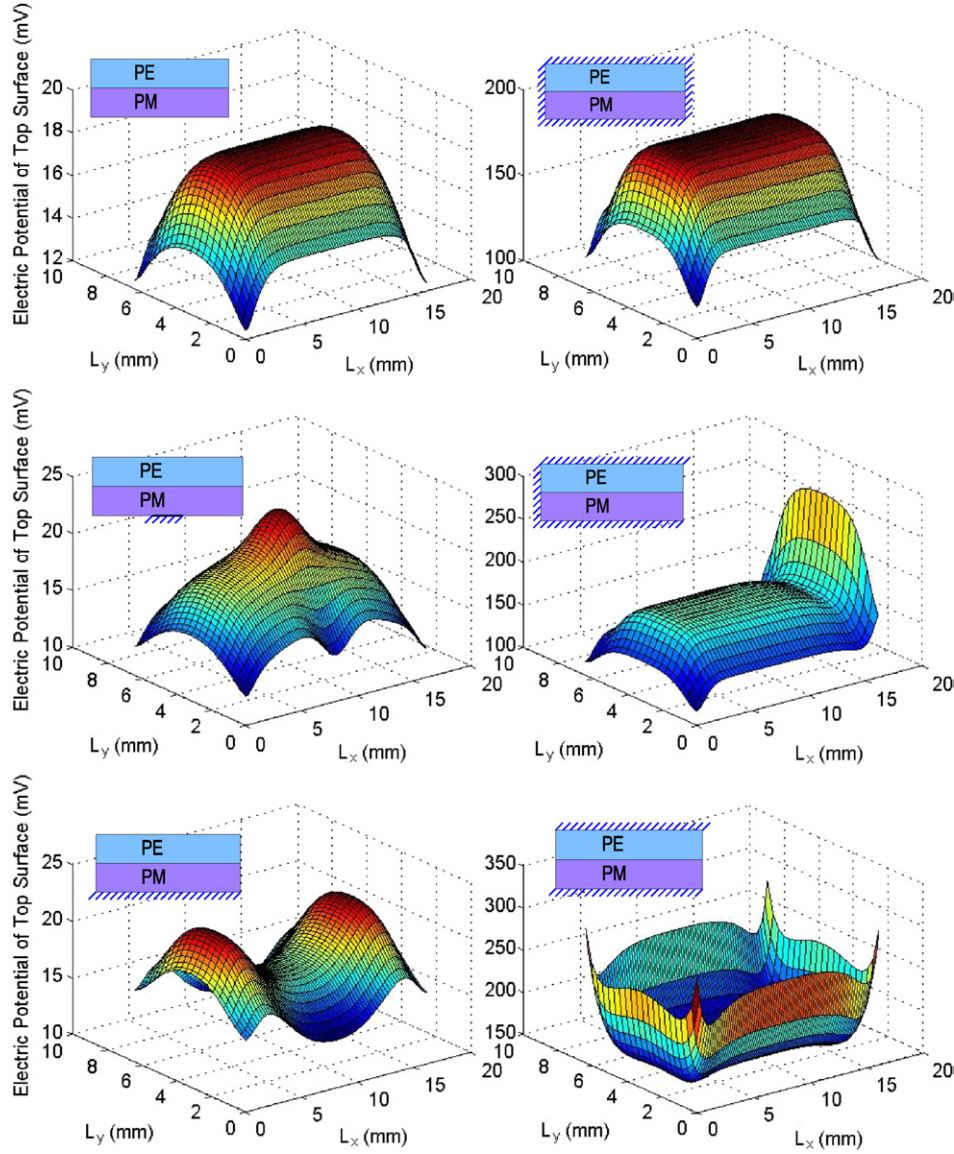


Figure 2. Electric potential distribution on the top surface of the bilayer PE/PM multiferroic composite under six different mechanical BCs (top to bottom on the left-hand side: BCs 1 to 3; top to bottom on the right-hand side: BCs 4 to 6). The electric and magnetic BCs are for the out-of-plane longitudinal case in figure 1(b) without using the electrode surface. (Colour online.)

where N_i ($i = 1-8$) are the shape functions. The shape functions are constructed in the elemental isoparametric coordinate and then transformed to the global coordinate by using the Jacobian matrix.

Considering the principle of virtual work

$$\int_V \bar{\sigma}^T \delta \bar{\gamma} dv = \delta \bar{u}^T F_e \quad (11)$$

in terms of the discretized extended nodal force and displacement vectors, we finally arrived at the following linear algebraic equations between the extended nodal force vector F_e and displacement vector \bar{u} .

$$F_e = K_e \bar{u}, \quad (12)$$

where K_e is the extended stiffness matrix in the discretized system, i.e.

$$K_e = \int_V \bar{B}^T \bar{D} \bar{B} dv. \quad (13)$$

3. Numerical modelling

To study the size and mechanical BC effect on the ME coupling, the common bilayer multiferroic composite is selected (figure 1(a)): the top layer is PE PZT-5A while the bottom layer is PM material CoFe_2O_4 , with their material properties listed in table 1 [6, 13, 25, 26]. The dimensions of this composite are defined by four geometric lengths: the two lateral dimensions in the x - and y -directions, L_x and L_y , and the thickness of the PE and PM layers, t_e and t_m . The electric and magnetic BCs are shown in figures 1(b) and (c). For figure 1(b), the magnetic field is created by applying a magnetic potential of 0.1 A on the top surface of the PM layer while keeping its bottom surface at 0 A. The electric potential on the bottom surface of the PE layer is set to zero while the unknown voltage on the top surface of the PE layer will be solved. Since the applied magnetic field and the unknown electric field are both along the vertical z -direction, this is

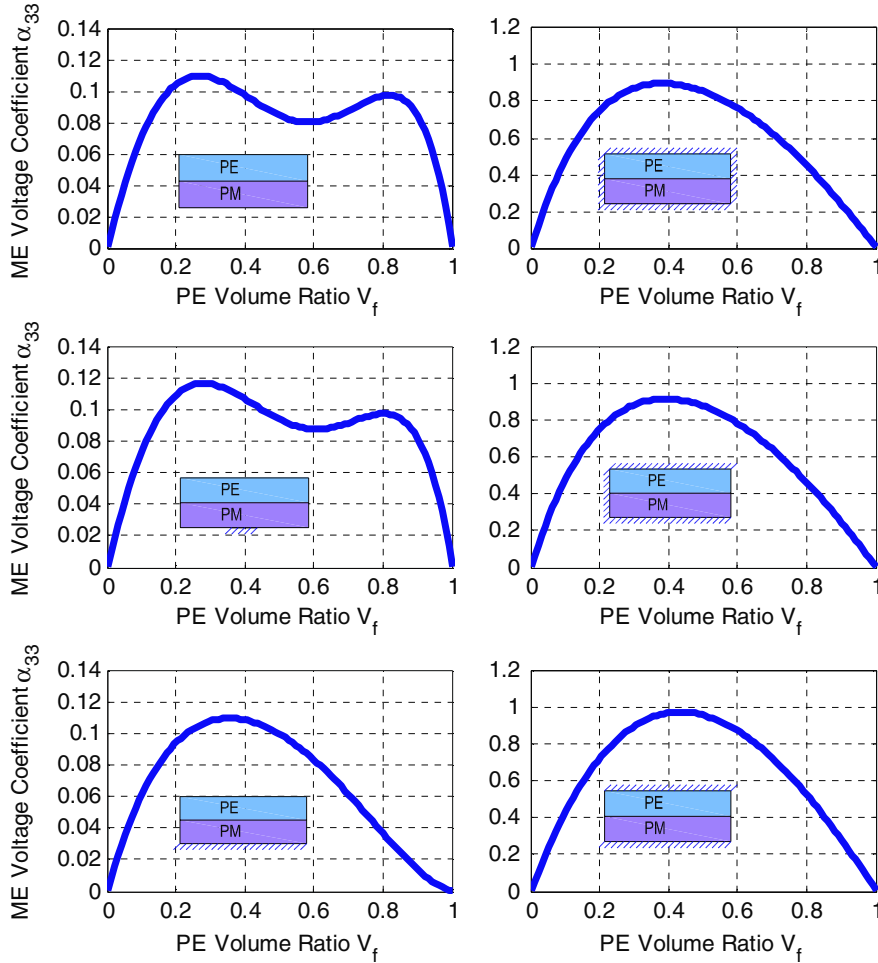


Figure 3. Variation of the ME voltage coefficient α_{33} versus volumetric ratio of the PE layer [$v_f = t_e / (t_e + t_m)$] of the bilayer PE/PM multiferroic composite under six different mechanical BCs (unit of α_{33} is $(V m^{-1})(A m^{-1})^{-1}$; top to bottom on the left-hand side: BCs 1 to 3; top to bottom on the right-hand side: BCs 4 to 6). The electric and magnetic BCs are for the out-of-plane longitudinal case figure 1(b) using the electrode surface conditions. (Colour online.)

sometimes called the out-of-plane longitudinal ME effect [8]. For figure 1(c), we apply a magnetic potential of 1.6 A on the left end of the PM layer while keeping its right end at 0 A. The electric potential on the left end of the PE layer is set to zero whilst the unknown voltage on the right end of the PE layer will be solved. Since the applied magnetic field and the unknown electric field are both along the horizontal x -direction, this is sometimes called the in-plane longitudinal ME effect [8]. In experiment, the magnetic field input can be achieved by using an electromagnet and a signal generator [27]. Thus, the input magnetic field is $H_z = 0.1/t_m$ (in the thickness or vertical direction) for the out-of-plane longitudinal case and $H_x = 1.6/L_x$ (in the longitudinal or horizontal direction) for the in-plane longitudinal case. Note that in general the permeability coefficient is not a constant but dependent on the bias magnetic field. In this study, we actually consider the incremental magnetic and electric fields, and therefore the permeability coefficient could be assumed to be constant if the incremental magnetic field is smaller than 1.5 Oe (about $120 A m^{-1}$) [9].

In our study, an actual device size was used with $L_x = 16 mm$, $L_y = 6.4 mm$ and $t_e = t_m = 1 mm$ [28], and furthermore six different mechanical BCs are considered.

They are classified as (see insets in figure 2): (1) BC1: all surfaces are traction-free; (2) BC2: all surfaces, except for a small fixed or clamped area on the bottom surface (1/25 of the total bottom length), are traction-free; (3) BC3: the bottom surface is clamped while others are traction-free; (4) BC4: all surfaces are clamped; (5) BC5: all surfaces, except for the right traction-free one, are clamped; (6) BC6: both the top and the bottom surfaces are clamped while others are traction-free. Again, our 3D FEM program has been verified via different approaches, and in the following examples a relatively refined mesh size was chosen to ensure that our 3D FEM prediction is accurate ($\sim 5\%$).

3.1. Effect of mechanical BCs and volumetric ratios

The FEM predicted electric potential contour distributions on the top surface of the PE layer (without electrode surfaces) for the out-of-plane longitudinal case (figure 1(b)) are shown in figure 2 for the six different mechanical BCs. It is clearly observed that:

- (1) While the voltage corresponding to BC1–BC3 are basically at the same magnitude, that to the BC4–BC6

is also at the same magnitude. However, the voltage magnitude to BC4–BC6 (right column) is about 10 times greater than that to BC1–BC3 (left column). This special feature is actually consistent with the result by a different analytical model and it is due to the induced large mechanical force on the clamped boundary [8].

- (2) Different mechanical BCs will induce different voltage distributions on the surface of the PE layer. For example, in the case of BC2, there is an obvious increment on the electric voltage right above the small clamped area. This is because at the position close to the clamped area, the mechanical deformation is constrained and the elastic stress is greater than those at other locations, resulting in a larger electric potential.
- (3) BC4 corresponds to a plate with all six surfaces being clamped. If one of the four lateral sides is released (BC5), the resulting electric potential along that side (or edge) will be substantially increased; if all the four lateral sides are released (BC6), then the voltages around these four sides (edges) are all increased.
- (4) Besides the six mechanical BCs discussed above, many other different mechanical BCs are investigated. It is found that the models with both the top and bottom surfaces being clamped can produce much larger electric potential (about 10 times larger) than other cases.

In the actual experimental setup, the top and bottom surfaces of the PE layer will be covered by the electrodes (with, of course, equal electric voltage) [9, 27]. Therefore, we also modified our 3D FEM program for this case and calculated the variation of ME voltage coefficients with different volume ratios of PE and PM phases. Based on the ME definition, we first have $\alpha_{33} = E_z/H_z$ ([8]), where E_z denotes the electric field across the whole thickness of the plate $E_z = V/(t_e + t_m)$ ([25]) with V being the uniform electric potential at the top surface. Figure 3 shows the variation of the ME voltage coefficient α_{33} in $(\text{V m}^{-1})(\text{A m}^{-1})^{-1}$ versus volumetric ratio of the PE layer ($v_f = t_e/(t_e + t_m)$) for the out-of-plane longitudinal case (figure 1(b)). While the lateral dimensions are kept the same (i.e. $L_x = 16 \text{ mm}$ and $L_y = 6.4 \text{ mm}$), we vary the volumetric ratio of the PE layer, $v_f = t_e/(t_e + t_m)$, from 0 to 1. It is apparent that $v_f = 0$ and $v_f = 1$, respectively, correspond to the single-phase PM and PE material case, and thus the ME coupling coefficient $\alpha_{33} = 0$.

From the top to the bottom on the left-hand side of figure 3 are the results for the mechanical BCs 1 to 3 and from top to bottom on the right-hand side are the results for the BCs 4 to 6. Similar to what we discussed for the electric potential distribution on the top surface of the PE layer, here, it is clearly observed that the ME coefficient for the mechanical BCs 4 to 6 is one magnitude larger than that for the mechanical BCs 1 to 3. It is further noticed that while for BCs 4 to 6 the maximum ME effect is reached around volumetric ratio $v_f = 0.4$, for the mechanical BCs 1 to 2, one observes two extremes in the ME value with magnitudes comparable to each other. This double-humped curve feature is due to the traction-free or near traction-free BC, with the result very close to the recent analytical prediction (figure 2, homogeneous NZFO in [11]). Furthermore for BC6, we point out that our result

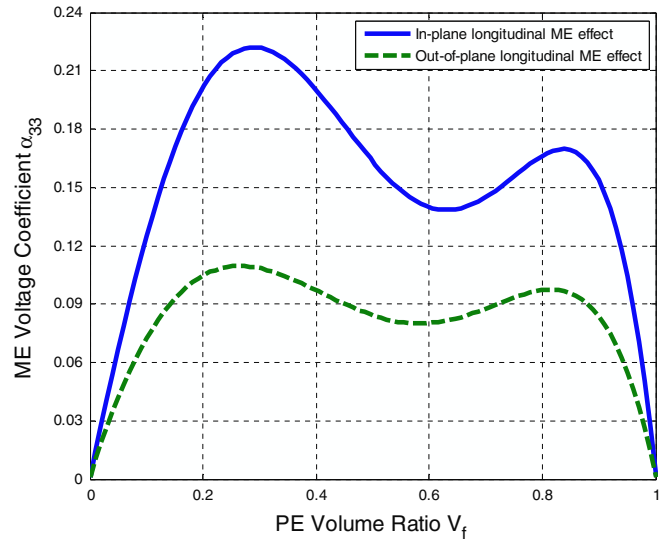


Figure 4. Comparison of the out-of-plane (figure 1(b)) and in-plane (figure 1(c)) longitudinal ME voltage coefficient α_{33} versus volumetric ratio of the PE layer [$v_f = t_e/(t_e + t_m)$] of the bilayer PE/PM multiferroic composite under BC BC1 with also the electrode surface conditions (unit of α_{33} is $(\text{V m}^{-1})(\text{A m}^{-1})^{-1}$). (Colour online.)

also coincides with the simple analytical solution (figure 5, $k = 1$ in [8]) (Note that the unit $(\text{V m}^{-1})(\text{A m}^{-1})^{-1}$ is about 800 times of $(\text{mV cm}^{-1}\text{Oe}^{-1})$), as will be discussed further in figure 6.

While the ME effect in figure 3 is based on the electrode surface condition, we point out that, actually, the electric potential distribution in figure 2 can also be utilized to find the ME voltage coefficient. Similar to the electrode surface case, the electric field across the whole thickness of the plate is calculated by $E_z = V_{\text{ave}}/(t_e + t_m)$, with V_{ave} being the average electric potential. Since the electric potential is different at different locations on the surface of the PE layer (figure 2), the average voltage over the surface is therefore used. It is very interesting that the ME voltage coefficient α_{33} based on this average surface electric potential method (with non-electrode surfaces) is nearly identical to that based on the electrode surface condition. In other words, the ME voltage coefficient curves based on the non-electrode condition will overlap those presented in figure 3. However, the electrode surface condition case would usually need more computational time as compared with the non-electrode one.

What we presented in figure 3 is the out-of-plane longitudinal ME effect (based on figure 1(b)). For the in-plane longitudinal case shown in figure 1(c), we have also calculated the corresponding ME effect for the mechanical BC BC1. Note that for the out-of-plane longitudinal case, the induced electric field is calculated with respect to the whole thickness of the bilayer, instead of the PE layer only. Thus, to make the results comparable to each other, we also calculate the induced in-plane electric field in the in-plane longitudinal case using the same thickness factor, i.e. $E_x = (V/L_x)t_e/(t_e + t_m)$. Figure 4 shows such a comparison for the traction-free BC1, and it is observed clearly that the in-plane longitudinal ME effect is much larger than the out-of-plane ME one.

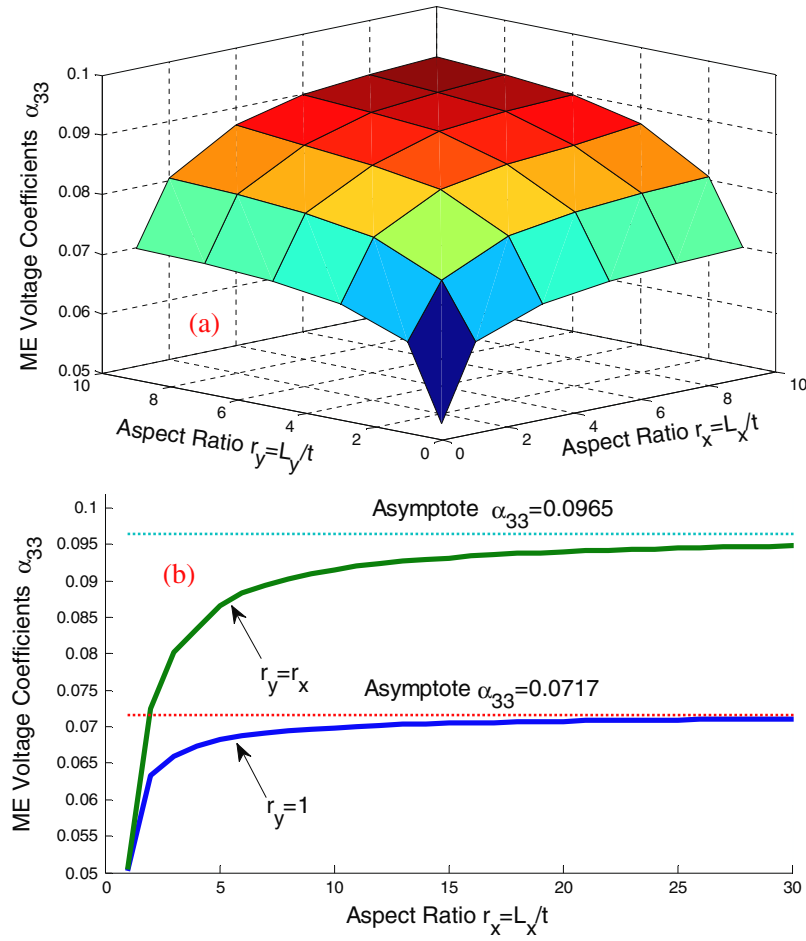


Figure 5. Variation of the ME voltage coefficient α_{33} versus lateral aspect ratios of the bilayer PE/PM multiferroic composite under the mechanical BC BC1 (unit of α_{33} is $(\text{V m}^{-1})(\text{A m}^{-1})^{-1}$): 3D contours in (a) and line variations with asymptotes in (b). The electric and magnetic BCs are for the out-of-plane longitudinal case in figure 1(b) with also the electrode surface conditions. (Colour online.)

3.2. Effect of aspect ratios

Besides the important influence of the mechanical BCs on the ME effect, the relative aspect ratio between the lateral dimension and the thickness of the multiferroic composites can also affect the ME coupling significantly. To show this, we also take the traction-free mechanical BC1 and out-of-plane longitudinal ME effect as an example. Results for the mechanically clamped case, such as BC6, show a similar trend but with an ME effect 10 times larger than that in BC1. We let the total thickness of the composite plate $t = t_e + t_m$ be a constant and further fix the volumetric ratio (i.e. $t_e/t_m = 1$). The two aspect ratios are defined as $r_x = L_x/t$ and $r_y = L_y/t$. The calculation is based on the electrode surface condition although the non-electrode case produces the same results.

The 3D contour of the ME voltage coefficient α_{33} versus the lateral aspect ratios ($r_x = L_x/t$ and $r_y = L_y/t$) of the bilayer PE/PM multiferroic composite (α_{33} in $(\text{V m}^{-1})(\text{A m}^{-1})^{-1}$) is shown in figure 5(a). It is obvious that since the polar axes of the PE and PM materials are along the z -direction (the thickness direction), α_{33} is symmetric about the diagonal line $r_x = r_y$. We also observe that with an increasing aspect ratio r_x or r_y , or both, the ME coefficient α_{33} gradually increases from 0.05 to 0.1. However, once the aspect ratio

reaches 15, the ME effect α_{33} increases very slowly. In other words, the ME coefficient α_{33} is approaching its asymptotic value when r_x and/or r_y becomes very large, an interesting feature similar to the recent experimental observation [29]. Figure 5(b) shows α_{33} as a function of r_x where the two solid lines are for the cases of $r_y = 1$ and $r_y = r_x$. These two lines are, respectively, taken along the side edge ($r_y = 1$) and the diagonal of the surface contour in figure 5(a) but are further extended to large aspect ratio r_x . It is clear that after r_x reaches 15, the magnitude of the two curves increases only slightly and gradually approaches their asymptotes, which are, respectively, $\alpha_{33} = 0.0717$ and 0.0965 . Therefore, while a large aspect ratio corresponds to a large ME effect, an aspect ratio around 15 should represent the highest possible ME effect (there is only less than 5% ME effect left in the large aspect ratio domain $r_x > 15$). Furthermore, figure 5(b) shows clearly that a composite plate ($r_x = r_y = 15$) will produce 20–30% higher ME coefficient than a composite beam ($r_x = 1; r_y = 15$).

While we have double checked our 3D FEM using different approaches (i.e. for a given problem, we used different mesh grids to test the convergence of the solution), we have also compared our numerical result with existing analytical solution. Figure 6 shows the comparison of the ME voltage coefficient α_{33} versus lateral aspect ratios between the present

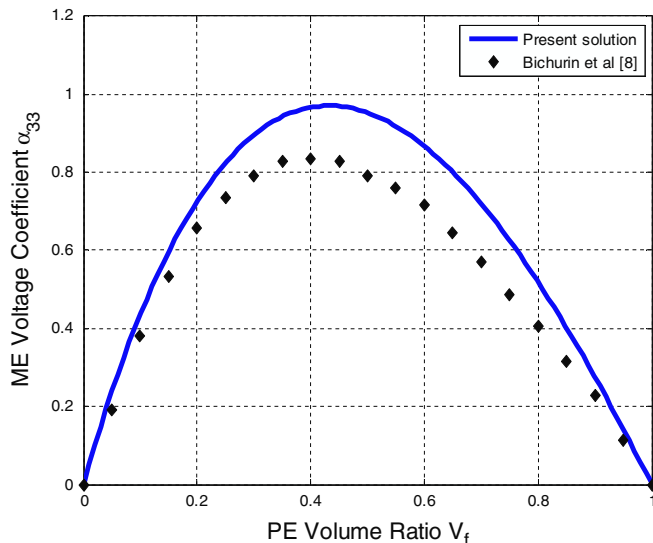


Figure 6. Variation of the ME voltage coefficient α_{33} versus lateral aspect ratios of the bilayer PE/PM multiferroic composite under the mechanical BC BC6 (unit of α_{33} is $(\text{V m}^{-1})(\text{A m}^{-1})^{-1}$): Present 3D FEM using the electrode surface conditions versus analytical solution [8] for the out-of-plane longitudinal case in figure 1(b). (Colour online.)

3D FEM using the electrode surface conditions and the analytical solutions [8] for the out-of-plane longitudinal case in figure 1(b) with the mechanical BC BC6. For this comparison, we have used different and large mesh sizes to approximate the infinite plate model used in [8]. It is noted that our FEM solutions not only converge to the curve shown in figure 6, as one could expect by examining figure 5, but also very close to the analytical one from [8]. The slight difference between our 3D FEM and the analytical results could be due to certain oversimplifications in the analytical model which will be investigated in the future (actually, the assumption on the horizontal stress behaviour over the thickness direction is incorrect in most analytical models).

4. Conclusion

In conclusion, we have developed a unique 3D FEM program for predicting the (out-of-plane and in-plane) ME effect in multiferroic composites and compared our results with recent analytical and experimental ones. Our program can deal with both the electrode and non-electrode surface conditions. Based on a typical bilayer PE/PM composite model, we have shown that: (1) the electric potential on the PE surface induced by the magnetic potential in the PM layer is not uniform but exhibits concentration near the edge/corner of the plate (without using the electrode surface condition); (2) the mechanically clamped BC can substantially enhance the ME effect; (3) the ME effect in a composite plate is stronger than that in the corresponding composite beam; (4) a large aspect ratio between the lateral dimension and the thickness of the composite plate corresponds to an enhanced ME effect; (5) the in-plane longitudinal ME effect is larger than the

out-of-plane longitudinal one; (6) the average electric potential on the surface of a PE layer without the electrode surface is almost identical to that based on the electrode surface condition. These results should be useful in the design of bilayer multiferroic composites.

Acknowledgment

This work was partially supported by the Air Force Office of Scientific Research under grant AFOSR FA9550-06-1-0317. The authors further thank the three anonymous reviewers for their very constructive comments.

References

- [1] Lal H B, Srivastava R and Srivastava K G 1967 *Phys. Rev.* **154** 505
- [2] Hornreich R and Shtrikman 1967 *Phys. Rev.* **161** 506
- [3] Yuan G L, Or S W, Liu J M and Liu Z G 2006 *Appl. Phys. Lett.* **89** 052905
- [4] Zheng H *et al* 2004 *Science* **303** 661
- [5] Fiebig M 2005 *J. Phys. D: Appl. Phys.* **38** R123
- [6] Nan C W 1994 *Phys. Rev. B* **50** 6082
- [7] Bichurin M I, Petrov V M and Srinivasan G 2002 *J. Appl. Phys.* **92** 7681
- [8] Bichurin M I, Petrov V M and Srinivasan G 2003 *Phys. Rev. B* **68** 054402
- [9] Dong S, Li J F and Viehland D 2003 *IEEE Trans. Ultrason. Ferroelectr. Freq. Control* **50** 1253
- [10] Dong S, Zhai J, Li J F and Viehland D 2006 *Appl. Phys. Lett.* **89** 243512
- [11] Petrov V M and Srinivasan G 2008 *Phys. Rev. B* **78** 184421
- [12] Wang X, Pan E, Albrecht J D and Feng W J 2009 *Compos. Struct.* **87** 206
- [13] Pan E 2001 *J. Appl. Mech.* **68** 608
- [14] Pan E and Heyliger P R 2002 *J. Sound. Vib.* **252** 429
- [15] Lalein V M, Petrov V M, Tuskov D S and Srinivasan G 2008 *Tech. Phys. Lett.* **34** 83
- [16] Popov C, Chang H, Abraham E, Whatmore R W and Huang Z 2008 *J. Electroceram.* **20** 53
- [17] Shi Z, Nan C W, Zhang J, Cai N and Li J F 2005 *Appl. Phys. Lett.* **87** 012503
- [18] Lu X Y, Wang B, Zheng Y and Ryba E 2007 *Appl. Phys. Lett.* **90** 133124
- [19] Lage R G, Soares C M M, Soares C A M and Reddy J N 2004 *Comput. Struct.* **82** 1293
- [20] Bhangale R K and Ganesan N 2006 *Int. J. Solids Struct.* **43** 3230
- [21] Ramirez F, Heyliger P R and Pan E 2006 *Mech. Adv. Mater. Struct.* **13** 249
- [22] Liu G, Nan C W, Cai N and Lin Y 2004 *Int. J. Solids Struct.* **41** 4423
- [23] Blackburn J F, Vopsaroiu M and Cain M G 2008 *J. Appl. Phys.* **104** 074104
- [24] Hinton E and Owen D R J 1977 *Finite Element Programming* (London: Academic)
- [25] Chang C M and Carman G P 2008 *J. Intell. Mater. Syst. Struct.* **19** 1271
- [26] Vel S S and Batra R C 2000 *AIAA J.* **38** 857
- [27] Nan C W, Cai N, Shi Z, Zhai J, Liu G and Lin Y 2005 *Phys. Rev. B* **71** 014102
- [28] Dong S and Viehland D 2006 Personal communications regarding a bilayer device sample
- [29] Ma J, Shi Z and Nan C W 2008 *J. Phys. D: Appl. Phys.* **41** 155001